Electronic and optical properties of superhard nanocomposite films obtained from C_{60} ion beam

2014 Mater. Res. Express 1 035049

(http://iopscience.iop.org/2053-1591/1/3/035049)

Materials Research
Express

Electronic and optical properties of superhard nanocomposite films obtained from C_{60} ion beam

V E Pukha[1,3], V L Karbovskii[2], S O Rudchenko[1], A N Drozdov[1], M V Maleyev[1], V V Starikov[1] and A T Pugachov[1]

[1] National Technical University (Kh.P.I), 21, Frunze Str., Kharkiv 61002, Ukraine
[2] Kurdyumov Institute of Metal Physics NASU, Kiev-142, 03680, Ukraine
E-mail: puch@kpi.kharkov.ua and vpukha@yandex.ru

Received 4 July 2014
Accepted for publication 7 August 2014
Published 25 September 2014
Materials Research Express **1** (2014) 035049
doi:10.1088/2053-1591/1/3/035049

Abstract

The study of electronic and transport properties of amorphous and nanocomposite superhard carbon films deposited from the mass-separated beam of accelerated C_{60} ions with an energy of 5 keV onto a substrate with temperatures (Ts) ranging from 373 K to 773 K is present. The films demonstrate a transition from the amorphous state with sp^2 2D clusters to nanocomposite one with 3D graphite nanocrystals at Ts ~ 573 K. That is accompanied by the registration of two phases with optical gaps of 3.6 eV and <1 eV. The narrow optical gap (<1 eV) is shown to attribute to the graphite nanocrystals, and a wide one (3.6 eV) to the amorphous diamond-like matrix. Measurement of the electrical conductivity of films at low temperatures showed a gradual transition at Ts increasing from hopping conductivity with variable length of jump in amorphous films to the tunnel one with power-law dependence from temperature for the nanocomposite and further to the percolation conductivity at direct contact of graphite nanocrystals. The role of intergranular insulator at tunneling conductivity of nanocomposite is played by amorphous carbon matrix which has an electronic structure close to amorphous diamond.

Keywords: nanocomposite, amorphous diamond, ion C_{60}, DLC, conductivity, power law

1. Introduction

The properties of amorphous carbon films and, therefore, the field of their application are determined essentially by ratio of sp^3 and sp^2 hybrids. Films with high content of sp^3 bonds (ta-

[3] Author to whom any correspondence should be addressed.

C films) due to high hardness, low friction coefficient, chemical passivity and biocompatibility are finding increasing industrial acceptance as protective and hardening coatings in automotive, aerospace and medical applications [1–5]. The unique properties of ta-C films have found different applications in electronic engineering. Electronic and optical properties of these films have allowed the creation of transistors, photovoltaic converters, light emitting diodes and memory cells [6–10]. The mechanical strength of films and high level of compression stresses are used for designing silicon devices with heightened carrier mobility [11].

Besides sp^3-to-sp^2 ratio, the electronic and the optical properties are influenced by substructural features of carbon films. These are sp^2 hybrid clusters and their orientation with regard to the surface, the presence of layered structures etc [12–13]. The increased content of an sp^2 fraction can be evident in the appearance of graphite nanocrystals. The presence of two phases, one of which may enclose another [14], can bring about the formation of films with nanocomposite structure. Usually for films deposited from single carbon ions the mechanical properties are degraded with decrease of sp^3 fraction. In particular, the hardness of such nanocomposite films can be well below that for ta-C [1]. The electric resistance of nanocomposites drops when quantity and dimension of graphite nanocrystals increase and finally approaches the resistance of crystalline graphite [15, 16].

The use of the accelerated C_{60} ions makes it possible to obtain a new type of superhard carbon films with hardness of ~50 GPa which practically does not degrade during transition from the amorphous state to nanocomposites [17–19]. At the same time the electrical conductivity of nanocomposites increases by 6 orders of magnitude compared to amorphous films and amounts to $\sim 10^3$ S/м. [18]. Thus, the use of accelerated fullerene ions for deposition of coatings allows varying over a wide range the electrical properties of films saving the high level of their mechanical properties.

It was earlier shown [20] that the electronic properties and conduction mechanisms of carbon nanocomposites obtained from C_{60} ion beam are similar to those of granulated metals. Possibilities of practical applications of granular structures to create microwave tunnel diodes, single-electron transistors, strain gauges etc are demonstrated in [21–24]. However, the electronic properties of the films obtained from the accelerated C_{60} ions and their relation to the structural state is still not understood.

In this paper we present the results of studying electronic and optical properties of carbon films of a new type by measuring electric resistance at low temperature and optical spectra. The correlation between different conduction mechanisms and the structure of films is established. The results show uniqueness of electronic and transport properties of films that enables expanding fields of carbon film application in electronic and optical instruments.

2. Experiments

As the basic material, fullerene C_{60} dust with purity of 99.5% (NeoTechProduct, St. Petersburg, Russia) was used. The ion beam was generated using a source with saddle electrical field. The discharge was ignited in fullerene vapor at accelerating voltage of 6 kV. From a source chamber the ion beam was directed into a magnetic mass separator and further on a substrate. In detail, an installation and a method of film deposition are described in [18, 19].

To deposit films the single-charged ions with mean energy of 5 keV and a dispersion of 1 keV were used. A rectangular aperture at an output of a mass-spectrometer spatially limited

the ion beam and produced mono-charged particle flux. During deposition the substrate holder moved back and forth across the ion beam with a step motor to increase the film area and improve its uniformity.

Two types of substrates were used: Si (100) and Al_2O_3 single-crystal wafers. In the process of deposition they could be heated to temperatures (T_S) of 100 up to 500 °C. Deposition rate was ~0.1 nm s^{-1}, and thicknesses of studied films were ~120 and ~300 nm.

2.1. Technique of research of nanocomposite coatings

The dependence of electrical resistance on temperature was measured by four-probe method from room temperature down to a temperature of liquid nitrogen. In this case carbon film was deposited through a mask on the alumina surface, and then Ag contacts were condensed on the film surface by vacuum evaporation.

Raman measurements were performed in backscattering geometry using JY LabRam HR fitted with liquid-nitrogen cooled CCD detector. The spectra were collected under ambient conditions using the 514.5 nm line of an argon-ion laser.

Optical properties of the films were investigated by double-beam spectrophotometer SF-26 in the wavelength range of $\lambda = 300$–1200 nm at room temperature. Spectra of optical transmission $T(\lambda)$ and reflectance $R(\lambda)$ were measured. To decrease the effect of Al_2O_3 substrate while monitoring $T(\lambda)$ spectra the Al_2O_3 substrate without film was placed in the comparison channel. Reflectance spectra $R(\lambda)$ were measured using an attachment device PZO-2 providing the double reflection of light from the experimental sample in comparison with reflection from the control sample.

Absorption of films for calculating E_g was obtained taking into account transmission and reflection spectra using the following expression:

$$\alpha = -\frac{1}{d}\ln\left(\frac{1}{R^2}\left(-\frac{(1-R)^2}{2T} + \sqrt{\frac{(1-R)^4}{4T^2} + R^2}\right)\right)$$

where d is the film thickness. The energy gap that corresponded to absorption coefficient 10^4 (E_{04}) was determined for substrate temperatures above 473 K by extrapolation of absorption curve in low energy.

3. Results and discussion

3.1. Optical properties

3.1.1. Raman spectroscopy. Measurement of the optical properties was carried out under normal conditions. Raman spectra are typical of amorphous carbon and have broad bands located between 1200 and 1800 cm^{-1} and a band near 700–800 cm^{-1}. The spectra of films obtained at temperatures below 573 K and films obtained at substrate temperatures over 673 K differ substantially (figure 1). Positions of the D- and G-bands were determined by fitting with a Gaussian function. D peak corresponds to a 'breathing' benzene ring vibration mode (change of hexagon diameter). G mode occurs at vibrations sp^2 carbon chains and benzene rings of type stretching in one direction and compression in other ('stretch' mode). In the lower frequencies (700–800 cm^{-1}) an appearance of L band corresponds to the rotational vibrations in plane of

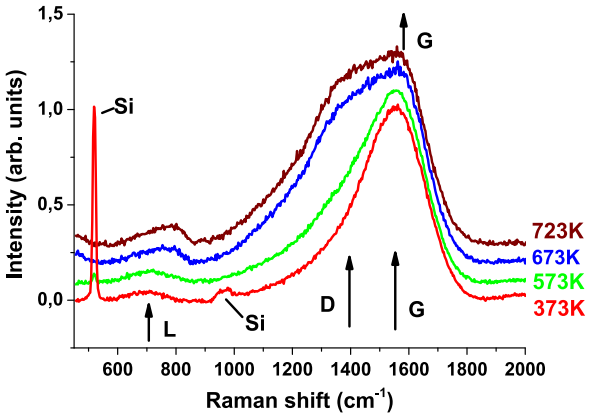

Figure 1. Raman spectra evolution with the substrate temperature (labeled at the right of curves). The arrows indicate positions of the L, D and G band centers. The features connected with dispersion from single-crystal Si substrate are visible in spectra of films prepared at low T_S.

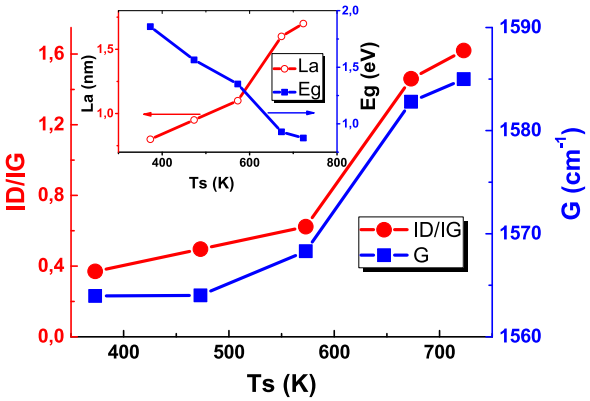

Figure 2. Intensity ratio of D and G bands (ID/IG) and shift of G band center versus T_S. In inset: the dependence of L_a, diameter of a cluster (correlation length in film plane) on deposition temperature T_S. E_g is band gap corresponding to the size of a graphite-like cluster.

benzene rings [25, 26]. The ratio of D and G band intensities and the shift of G band center versus T_S are shown in figure 2.

According to a model proposed by Ferrari and Robertson [25] successive change in ID/IG ratio from 0.4 to 1.6 and G band shifts from 1565 cm^{-1} to 1585 cm^{-1} indicate that the film presents nanographite with relatively low content of sp^3 bonds. Increase of the substrate temperature during deposition is usually accompanied by two processes: reduction of sp^3 bond content and clustering of the sp^2 phase, along with process of cluster ordering. These processes are usually separated in temperatures with the sp^2 clustering taking place at lower temperature.

For Raman spectra in visible range the clustering has the main influence on ID/IG ratio. Moreover, as shown in [25], this ratio can be used to estimate the size of sp^2 clusters (in the case of their small size <2 nm) by the formula:

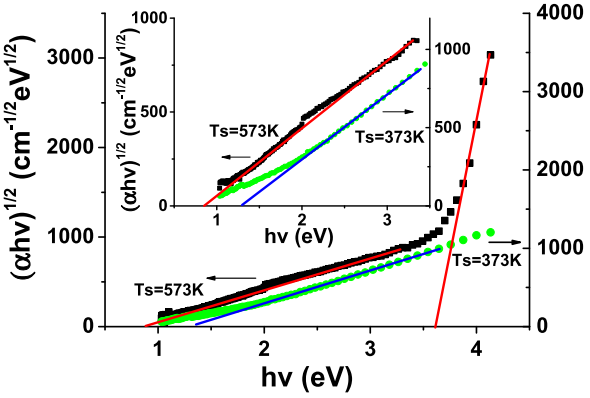

Figure 3. Tauc plots for different deposition temperatures *T*s of 373 K and 573 K. The tangents to the linear sections of the spectrum are drawn. The inset shows the low-energy part of the graph on a larger scale. The curves are in different scales with respect to $(\alpha hv)^{1/2}$ axis (corresponding axes of the graph are shown by arrows).

$$\frac{I(D)}{I(G)} = C'(\lambda)L_a^2,$$

where L_a is diameter of a cluster or correlation length in film plane; λ is exciting wavelength and $C'(514.5\,\text{nm}) = 0.55\,\text{nm}^{-2}$. An estimation gives typical values of graphite clusters within 0.8 −1.7 nm in the temperature range of 373–773 K. In other words, the size of nanocrystals increases with substrate temperature. In the range of 573–673 K the temperature dependence of average cluster size is the strongest and corresponds to variation of cluster sizes from 1.1 to 1.6 nm (figure 2, inset).

The results obtained from analysis of Raman spectra suggest the restructuring of the carbon films at $T_S \sim 573$–673 K. In addition to *I*D/*I*G jump and corresponding correlation length change, the step-wise shift of G band (figure 1) and separation of L band (~700 cm^{-1}) for two peaks (704 and 786 cm^{-1}) take place. The latter is difficult to interpret within the existing model framework [25]. The G peak movement is associated with disorder decrease and clustering of sp^2 hybrids. Disorder reduction can mean the film crystallization, that is, the appearance of nanocrystals. Indeed, at substrate temperatures between 573 and 673 K, as was shown in [18, 19], the reflection from (002) planes of graphite nanocrystals instead of halo appears in the microdiffraction patterns. Thus, jump of parameters identified by the analysis of Raman spectra corresponds to a transition from 2D clusters to 3D graphite nanocrystals.

3.1.2. Absorption spectra. At low deposition temperatures ($T_S \sim 373$–473 K) the optical absorption of deposited films is close to that usually observed for amorphous carbon films [27–30]. The energy gap E_{04}, corresponding to absorptance of 104 cm^{-1}, is 1.2–1.23 eV. Construction of Tauc plots (dependence of $(\alpha hv)^{1/2}$ from energy, figure 3) allowed determining width of Tauc gaps to be 1.3 and 1.25 eV for *T*s 373 and 473 K correspondingly.

The increase of substrate temperature leads to the appearance of absorption jump in the energy range close to 4 eV. In the Tauc plot there are two rectilinear segments: the first segment corresponds to a gap of less than 1 eV and the second one $E_g \sim 3.6$ and ~3.4 eV for Ts ~ 573 K and 673 K, correspondingly. The discovered transitions indicate composite structure of the sample. The wide-band-gap component of composite has optical gap E_g larger than that for

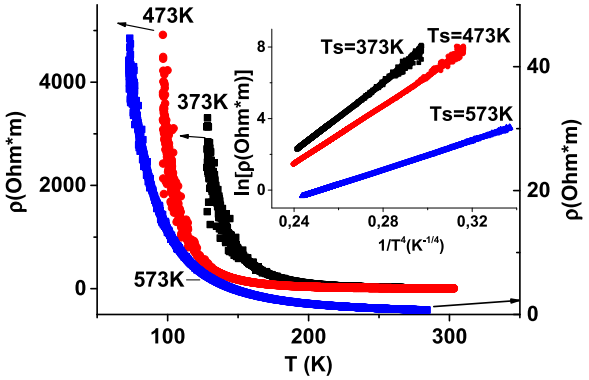

Figure 4. The temperature dependence of the resistivity (ρ) and a plot of the resistance logarithm ($\ln R$) versus temperature T with exponent (−1/4) (insert). The substrate temperature (Ts) designations during film deposition (Ts = 373, 473, 573 K) are near to each curve. The curves are plotted with different scales of resistivity (corresponding axis of the graph is shown by arrows).

Table 1. Tauc gap, E_{04}, and band gap E_g. corresponding to the size of La sp^2 formations depending on the deposition temperature Ts.

Ts, K	373	473	573	673
Tauc gap, eV	1.3	1.25	0.9 and 3.6	0.82 and 3.4
E_{04}, eV	1.23	1.2	0.9	0.77
L_a, nm	0.8	0.95	1.1	1.6
E_g, eV	1.8	1.5	1.3	0.9

diamond-like films with concentration of sp^3 hybrids 88% (3 eV [28]). In narrow-band-gap component the optical gap nonmonotonically decreases from 1.3 to 0.82 eV with increase of T_S. In the range of $T_S \sim 473–573$ K the optical gap drops from 1.25 to 0.9 eV (~30%). These changes, with some advance in temperature, correlate with a jump of Raman parameters that corresponds with the appearance of 3D graphite nanocrystals. We supposed that narrow-band-gap component is connected with 2D graphite-like clusters for low temperatures and 3D nanocrystals for high T_S. Graphite has no band gap but at small sizes of crystals (about nanometers) there is a band gap because of spatial quantization [28, 29]. The value of band gap E_g depends on quantity of hexagon cells M in graphen planes and, as shown in [31], decreases proportionally $M^{-0,5}$. In other words the band gap for graphitic formations is close to the value determined by the following equation:

$$E_g \approx 2\,|\beta|\,M^{-0.5},$$

where β is bond energy between π-orbitals of the nearest adjacent atoms (~2.9 eV). For perfect compact clusters consisting of benzene rings integrated in equiaxial 2D grid, the estimation of band gap width E_g is shown in the inset of figure 2. Tauc gap, E_{04} and band gap corresponding to size of sp^2 formations depending on deposition temperature are shown in table 1. The obtained estimations of E_g exceed slightly the values of E_{04} and Tauc gap obtained from absorption spectra. We consider it is connected to imperfections of the structure in graphite-like formations of the films. Besides, the presence of noncompact clusters can also reduce the observed width of optical band gap (for example, for linear clusters with $E_g \approx 2|\beta|M^{-1}$). The

presence of defects in sp^2 clusters is lowered with increase of Ts because of activation of diffusion processes during deposition process. Therefore, the difference between values obtained from absorption spectra and E_g is reduced with increase of T_S.

Thus, for elevated temperatures ($T_S \sim 473$–573 K) the component of the composite with narrow-band-gap (<1 eV) is the graphite nanocrystals while the component with wide-band-gap is an amorphous diamond-like matrix of nanocomposite [18]. Width of optical band gap ($T_{Eg} \sim 3.4$–3.6 eV) allows supposing that the amorphous nanocomposite matrix contains above 90% sp^3 bonds and is close to properties of amorphous diamond.

3.2. Electrical properties

The analysis of Raman spectroscopy data and optical absorption spectra shows that there is a transition from amorphous diamond-like structure to nanocomposite one in films obtained at T_S close to 573 K. There are 2D graphite-like clusters in amorphous structure which are converted to graphitic nanocrystals when T_S increases. It should be note that the nanocomposite matrix has wide optical band gap. Such films may have features of the transport properties during the flow of electric current in the case of both amorphous and nanocomposite structure of films.

The dependence of film resistance on T_S measured at room temperature (RT = 293 K) has 5-order drop for T_S ranging from 573 K to 723 K [18]. To determine the type and the mechanism of conductivity the dependence of electric resistance of films was measured from RT down to temperature of liquid nitrogen (figure 4). For all films decrease of conductivity with temperature is observed. In other words the films obtained in this temperature range have semiconductor properties. On the other hand, we can select three T_S ranges where the different mechanisms of charge transfer prevail. At low T_S (373–573 K) when films have amorphous structure [18, 19] the temperature dependence of resistance R is well described by an equation such as $R = R_0 \exp\ (T_0/T)^x$, where R_0 and T_0 are temperature-independent constants, T is temperature of resistance measurement and x is less 1. Such a relationship is characteristic for materials in which the charge transfer at low temperatures is carried out according to the mechanism of hopping conductivity with a variable range hopping.

For films deposited at temperatures of 373–573 K the exponent x is 1/4 (figure 4 inset), and conductivity behaviour is described by classic Mott law [32]. In this case T_0 is determined by density of localized states near to Fermi level N (E_F) and α^{-1} is radius of localized state of electron wave function [27]:

$$T_0 = 16\alpha^3/kN\left(E_F\right),$$

where k is Boltzmann constant.

Let us take that the radius of localized state is equal to characteristic dimension of graphite-like cluster, which is determined from the ratio of Raman band intensities ID/IG (table 1). The value T_0 is determined using linear adjustment of experimental data: $\ln R = \ln R_0 + (T_0/T)^{1/4}$. In this case it is possible to determine the density of localized states near to Fermi level $N(E_F)$ for each film. Table 2 shows the values of T_0, N (E_F) and the radii of the localized states α^{-1}, depending on the deposition temperature.

The density of states near to Fermi level $N(E_F)$ is proportional to concentration of nanoclusters which have levels near to center of energy gap E_g. As shown in [31] the defects such as pentagonal and heptagonal rings inserted in graphite grids and also grids with odd carbon atoms quantity give additional states near the center of band gap. The temperature rise of

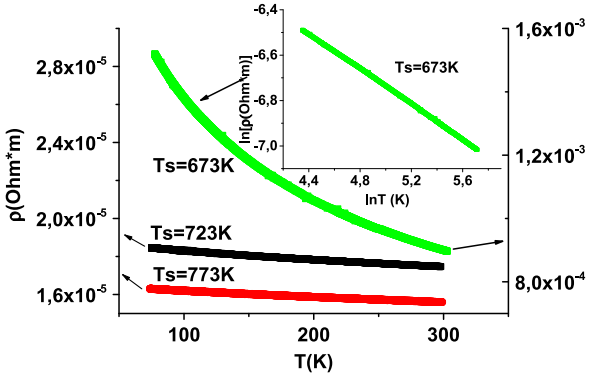

Figure 5. The temperature dependence of the resistivity (ρ) and plot of the resistance logarithm (ln$R$) versus ln$T$ (sample obtained at substrate temperature of 673 K). The substrate temperatures during deposition (Ts = 673, 723, 773 K) are near to each curve. The curves are in different scales resistivity (axis of the graph corresponding to the curves shown by arrows).

Table 2. Values of constant T_0, density of states $N(E_F)$ and localization radius α^{-1} for deposition temperatures $T_S = 373 - 573$ K.

T_S, K	T_0, K	$N(E_F)$, (eV cm^3)$^{-1}$	α^{-1}, nm
373	92 236 816	$2.14 \cdot 10^{16}$	0.8
473	47 917 406.6	$9.36 \cdot 10^{15}$	0.95
573	2798 293.3	$4.72 \cdot 10^{14}$	1.1

substrate leads to annealing of defect states and improvement of sp^2 structure formations (clusters) and causes decrease of levels density near to Fermi level. In addition to annealing of defect states there is a growth of sp^2 clusters and decrease of distance between them. In that case in addition to hopping conduction, another mechanism of charge transfer appears.

Rising Ts results in decreasing the slope in temperature dependence of resistance. The conductivity behavior of the films deposited at Ts > 573 K cannot be described by hopping conduction. Another conductivity mechanism becomes evident at Ts close to 673 K. These films also have semiconductor character in temperature dependence of resistance similar to films deposited at lower Ts. Resistance of films is larger by a factor of 1.8 times at a temperature of 77 K compared to RT (figure 5).

We could not adapt dependence $R = R_0 \exp(T_0/T)^x$ to experimental curve by varying R_0, x and T_0. Research of optical properties of films described in the present work and also structure research described in [18] have shown that the film is nanocomposite in which the sp^2 nanocrystals with narrow band gap (<1 eV) are enclosed in amorphous matrix with wide band gap (~3.5 eV).

The conductivity of granular metals having structure close to nanocomposite films is substantially realized due to the tunnel mechanism of charge transfer between metal grains. Thus, for 3D systems the temperature dependence of resistance has power law $R \sim R_0 T^{\alpha}$ or logarithmic nature $R = R_0 \ln(T_0/T)$ [33, 34]. We found that the experimental curve for resistance is close to an exponential function: $R = R_0 T^{\alpha}$. The reconstruction of the curve in ln$R$–ln$T$ coordinates (figure 5, inset) allowed the use of linear adjustment to determine the value of $\alpha = -0.386$ and to establish that the exponential dependence is kept in all intervals of measured

Table 3. The type of fitting equations for conductivity determination and its parameters against deposition temperature T_S. Values of temperature dependent component in the equation $\sigma_0 T^{-\alpha}$ at 100 and 293 K are also added.

Ts, K	Equation	σ_1, S m^{-1}	σ_0	α	$\sigma_0 T^{-\alpha}$ (100 K), S m^{-1}	$\sigma_0 T^{-\alpha}$ (293 K), S m^{-1}
673	$\sigma = \sigma_0 T^{-\alpha}$	~0	122	−0.386	722	1093
673	$\sigma = \sigma_1 + \sigma_0 T^{-\alpha}$	142	68	−0.466	581	952
723	$\sigma = \sigma_1 + \sigma_0 T^{-\alpha}$	51 942	152	−0.623	2668	5232
773	$\sigma = \sigma_1 + \sigma_0 T^{-\alpha}$	59 826	64.3	−0.736	1906	4205

temperatures from liquid nitrogen up to RT. Parameter α is connected with tunnel specific conductivity, and the power-mode law for temperature dependence of resistance in granular electronic systems works at high tunnel conductivity of intergranular isolator [22, 34].

Further increase of temperature ($T_S \sim 723$–773 K) results in thinning diamond-like matrix and originating percolation paths of conductivity with direct participation of graphite nanocrystals. Decrease of the slope for temperature dependence of resistance is also observed. The semiconductor character of resistance variation can be approximated by a function of $R = 1/(a + b \cdot T^c)$, where a, b and c are factors depending on T_S but not depending on temperature of resistance measurement. In this case the conductivity equation is of the form $\sigma = a + bT^c$. From the exponential function $R = R_0 T^{\alpha}$ obtained at $T_S = 673$ K it is evident that $\sigma = \sigma_0 T^{-\alpha}$. Thus, if we rename a, b and c as σ_1, σ_0 and α, the dependence of conductivity from temperature will be $\sigma = \sigma_1 + \sigma_0 T^{-\alpha}$. From the last equation it is followed that the power law for temperature dependence of resistance is saved even at $T_S \sim 723$–773 K when the resistivity of film drops below 1.6×10^{-5} Ohm · m. Thus, the additional paths of electric charge transfer occur, which are characterized by temperature-independent parameter indicated as σ_1 that gives the additive contribution to the film conductivity. We consider that parameter σ_1 is connected with percolation mechanism of conductivity and its value depends on the crystalline state of the film.

The fit for experimental dependence by equation $R = 1/(a + b \cdot T^c)$ was carried out to confirm existence of additional temperature-independent paths of charge transfer in the film deposited at Ts = 673 K. The high accuracy of the curve fitting revealed a small additive parameter being present at film conductance in this case. At room temperature its contribution makes ~13%. It gives appreciable contribution in film conductivity at low temperatures (~20% at 100 K). Parameters determining the conductivity of films obtained at $T_S \geqslant 673$ K can be seen in table 3.

Table 3 shows the parameter σ_1 increases more than 350 times with temperature and its contribution to the conductivity at $T_S = 723$ K makes ~90% even at room temperature. It should be noted that temperature dependent component $\sigma_0 T^{-\alpha}$ connected with specific tunneling conductance increases ~5 times in this range of T_S. Further T_S growth decreases $\sigma_0 T^{-\alpha}$ contribution in spite of an increase in absolute value of α. Difference in contributions of both temperature-dependent and temperature-independent component of conductivity is well agreed with structural changes accompanied in the film within the temperature range from 673 K to 723 K. The deposition temperature rise results in thinning diamond-like matrix that increases specific tunneling conductance between nanocrystals. On the other hand the contribution of tunneling conductance to general conductance is decreased at the expense of direct contact of graphite nanocrystals.

Thus, by changing the fabrication mode it is possible to form coatings with at least three different mechanisms of conduction, which correspond to the different structural states of the films. The most interesting among them is the films with the structure similar to the granular metals, making them attractive for application in electronic devices of a new generation.

4. Conclusion

We studied the electronic structure and transport properties of the superhard carbon films deposited from the mass separated beam of accelerated C_{60} ions ($E \sim 5$ keV) at substrate temperatures from 373 to 773 K. The analysis of Raman spectra and optical absorption of films has shown that transition from 2D clusters in amorphous film to 3D nanocrystals and nanocomposite film occurring at $T_S \sim 573$ K is accompanied by absorption jump in the region of energies close to 4 eV. It is shown that nanocomposite consists of both the narrow-band-gap component (optical gap < 1 eV) corresponding to graphite nanocrystals, and the wide-band-gap component (optical gap 3.6–3.4 eV) corresponding to amorphous diamond-like matrix. So large width of optical gap allows one to suggest that the amorphous matrix of nanocomposite contains over 90% of sp^3 bands and its properties are close to amorphous diamond.

Conductivity at low temperatures decreases with temperature for all films obtained within the substrate temperatures from 373 to 773 K. Three T_S subranges are revealed where different mechanisms of charge transfer prevail. At low T_S (373–573 K) when films have amorphous structure, charge transfer is determined by hopping conduction with variable length of jump. It is shown that for amorphous films the density of localized states near to Fermi level $N(E_F)$ drops by a factor of ~50 [from 2.14×10^{16} down to 4.72×10^{14} $(\text{eV cm}^3)^{-1}$] when T_S increases up to 573 K. Decrease of the film resistivity in this case takes place at the expense of growing radius of localized state of electron wave function connected with the size of sp^2 clusters.

Growth of deposition temperature up to 673 K results in the power law for the temperature dependence of conductivity which is characteristic for granular electronic systems and acts at high tunneling conductance of intergranular isolator. It is shown that in addition to the temperature-dependent charge transfer through the diamond-like interlayers between nanocrystals there is a temperature-independent component of conductivity with contribution increasing with deposition temperature (from 13% at $T_S = 673$ K to 95% at $T_S = 773$ K). We attribute the temperature-independent component of conductivity to originating of percolation paths of charge transfer with direct participation of graphite nanocrystals. The deposition temperature above 673 K results in thinning of diamond-like matrix and direct contact between graphite nanocrystals.

The features of optical spectra for nanocomposites and data on resistance measurement agree well with structural model offered in [18] (oriented graphite nanocrystals in amorphous diamond-like matrix). Using optical absorption spectra we have shown that the matrix of composite is close to properties of amorphous diamond.

References

[1] Robertson J 2002 *Mater. Sci. Eng. R.* **37** 281

[2] Donnet C and Erdemir A 2008 *Tribology of Diamond-Like Carbon Films. Fundamentals and Applications* (New York: Springer)

[3] Love C A, Cook R B, Harvey T J, Dearnley P A and Wood R J K 2013 *Tribol. Int.* **63** 141
[4] Robertson J 2010 *Diamond-Like Carbon for Applications in Industrial Plasma Technology: Applications from Environmental to Energy Technologies* (Weinheim: Wiley) p 277
[5] Bewilogua K, Bräuer G, Dietz A, Gäbler J, Goch G, Karpuschewski B and Szyszka B 2009 *CIRP Ann.-Manuf. Technol.* **58** 608–27
[6] Zhu H, Wei J, Wang K and Wu D 2009 *Sol. Energy Mater. Sol. Cells* **93** 1461
[7] Wu Y, Lin Y, Bol A A, Jenkins K A, Xia F, Damon B, Zhu F Y and Avouris P 2011 *Nature* **472** 74
[8] Fu D, Xie D, Feng T, Zhang C, Niu J, Qian H and Liu L 2011 *IEEE Electron Device Lett.* **32** 803
[9] Zhang L, Li Q, Dong Y and Ma Z 2012 *Optoelectron. Lett.* **8** 113
[10] Milne W I 2003 *Semicond. Sci. Technol.* **18** 81
[11] Tan K M, Zhu M, Fang W W, Yang M, Liow T Y, Lee R and Yeo Y C 2008 *IEEE Electron Device Lett.* **29** 192
[12] Carey J D and Silva S R P 2004 *Phys. Rev.* **70** 235417
[13] Carey J D 2006 *Thin Solid Films* **515** 996
[14] Cho N H, Veirs D K, Ager J W, Rubin M D, Hopper C B and Bogy D B 1992 *J. Appl. Phys.* **71** 2243
[15] Mounier E, Bertin F, Adamik M, Pauleau Y and Barna P B 1996 *Diam. Relat. Mater.* **5** 1509
[16] Chhowalla M, Robertson J, Chen C W, Silva S R P, Davis C A, Amaratunga G A J and Milne W I 1997 *J. Appl. Phys.* **81** 192
[17] Pukha V E, Pugachov A T, Churakova N P, Zubarev E N, Vinogradov V E and Nam S C 2012 *J. Nanosci. Nanotechnol.* **12** 4762
[18] Pukha V E, Zubarev E N, Drozdov A N, Pugachov A T, Jeong S H and Nam S C 2012 *J. Phys. D: Appl. Phys.* **45** 335302
[19] Penkov O V, Pukha V E, Zubarev E N, Yoo S S and Eun D 2013 *Tribol. Int.* **60** 127
[20] Pukha V E, Karbovskii V L, Drozdov A N and Pugachov A T 2013 *J. Phys. D: Appl. Phys.* **46** 485305
[21] Huth M 2010 *J. Appl. Phys.* **107** 113709
[22] Beloborodov I S, Lopatin A V, Vinokur V M and Efetov K B 2007 *Rev. Mod. Phys.* **79** 469
[23] Likharev K K 1999 *Proc. IEEE* **87** 606
[24] Durrani Z A K 2010 *Single-Electron Devices and Circuits in Silicon* (London: Imperial College Press)
[25] Ferrari A C and Robertson J 2000 *Phys. Rev.* B **61** 14095
[26] Rodil S E, Ferrari A C, Robertson J and Milne W I 2001 *J. Appl. Phys.* **89** 5425
[27] Hauser J J 1977 *J. Non-Cryst. Solids* **23** 21
[28] Teo K B K, Ferrari A C, Fanchini G, Rodil S E, Yuan J, Tsai J T H, Laurenti E, Tagliaferro A, Robertson J and Milne W I 2002 *Diam. Relat. Mater.* **11** 1086
[29] Vogel M, Stenzel O, Petrich R, Schaarschmidt G and Scharff W 1993 *Thin Solid Films* **227** 74
[30] Teo K B K, Rodil S E, Tsai J T H, Ferrari A C, Robertson J and Milne W I 2001 *J. Appl. Phys.* **89** 3706
[31] Robertson J and O'Reilly E P 1987 *Phys. Rev.* B **35** 2946
[32] Mott N F and Davis E A 1971 *Electronic Processes in Non-Crystalline Materials* 7 (Oxford: Clarendon press) p 55
[33] Gerber A, Milner A, Deutscher G, Karpovsky M and Gladkikh A 1997 *Phys. Rev. Lett.* **78** 4277
[34] Efetov K B and Tschersich A 2003 *Phys. Rev.* B **67** 174205